Experimentally realizable devices for controlling the motion of magnetic flux quanta in anisotropic superconductors

SERGEY SAVEL'EV[1] & FRANCO NORI*[1,2]

[1]Frontier Research System, The Institute of Physical and Chemical Research (RIKEN), Wako-shi, Saitama 351-0198, Japan
[2]Center for Theoretical Physics, Department of Physics, CSCS, University of Michigan, Ann Arbor, Michigan 48109-1120, USA
*e-mail: nori@umich.edu

A new generation of microscopic ratchet systems is currently being developed for controlling the motion of electrons and fluxons, as well as for particle separation and electrophoresis. Virtually all of these use static spatially asymmetric potential energies to control transport properties. Here we propose completely new types of ratchet-like systems that do not require fixed spatially asymmetric potentials in the samples. As specific examples of this novel general class of ratchets, we propose devices that control the motion of flux quanta in superconductors and could address a central problem in many superconducting devices; namely, the removal of trapped magnetic flux that produces noise. In layered superconductors there are two interpenetrating perpendicular vortex lattices consisting of Josephson vortices (JVs) and pancake vortices (PVs). We show that, owing to the JV–PV mutual interaction and asymmetric driving, the a.c. motion of JVs and/or PVs can provide a net d.c. vortex current. This controllable vortex motion can be used for making pumps, diodes and lenses of quantized magnetic flux. These proposed devices sculpt the microscopic magnetic flux profile by simply modifying the time dependence of the a.c. drive, without the need for samples with static pinning—for example, without lithography or irradiation.

New microscopic ratchet systems[1–9] are currently being developed for controlling the motion of particles. The controlled transport of magnetic flux quanta in superconductors[7–9] could be very useful for designing micromagnetic flux quanta machines such as magnetic flux pumps, diodes and lenses in order to create desired magnetic profiles within the sample or device. In contrast with many other systems, the density of magnetic vortices as well as the strength and range of their interaction can be easily modified by an external magnetic field and temperature. This 'tunability' of vortex arrays gives rise to very rich equilibrium and non-equilibrium properties[10–15] and makes them ideally suited for regulating the motion of magnetic flux quanta. However, the potential-energy landscape where vortices move is usually disordered, hard to manipulate, and permanently fixed after the sample is fabricated; limiting the degree of control on the motion of flux quanta. Therefore, it would be greatly desirable to have a much more adjustable and malleable pinning landscape. This can be realized for vortices in strongly anisotropic layered superconductors such as $Bi_2Sr_2CaCu_2O_{8+\delta}$.

Direct visualization[16–20] as well as magnetic[21] and transport[22,23] measurements clearly show that a magnetic field tilted away from the crystalline axis penetrates a strongly anisotropic layered superconductor as two interpenetrating vortex arrays, known as a crossing or combined vortex lattice[24,25]. One vortex sublattice consists of stacks of pancake vortices (PVs) aligned along the c axis, whereas the other sublattice is formed by Josephson vortices (JVs) confined between layers (Fig. 1). Superconducting currents generated by JVs deform stacks of PVs inducing their local inclination[25–28]. The energy of the curved pancake stack depends on its position with respect to the JV sublattice, causing PV–JV mutual pinning. This pinning has been experimentally observed[16–20] through the formation of PV chains alternating the regular triangular PV lattice in tilted magnetic fields.

In contrast with the usual random frozen pinning attributed to local inhomogeneities in the sample, the PV–JV pinning provides a periodic potential with a strength and spatial period which are easily changed by the in-plane magnetic field. Another remarkable feature of the crossing-lattice pinning is its mobility under the action of driving forces applied to the JV sublattice. For example, an applied d.c. current flowing along the c axis drives the JV sublattice, which, in turn, drags PVs, generating an in-plane d.c. electrical current and vice versa. In such a device with d.c. input and d.c. output, the velocities of both the PVs and JVs are the same, which leads to a
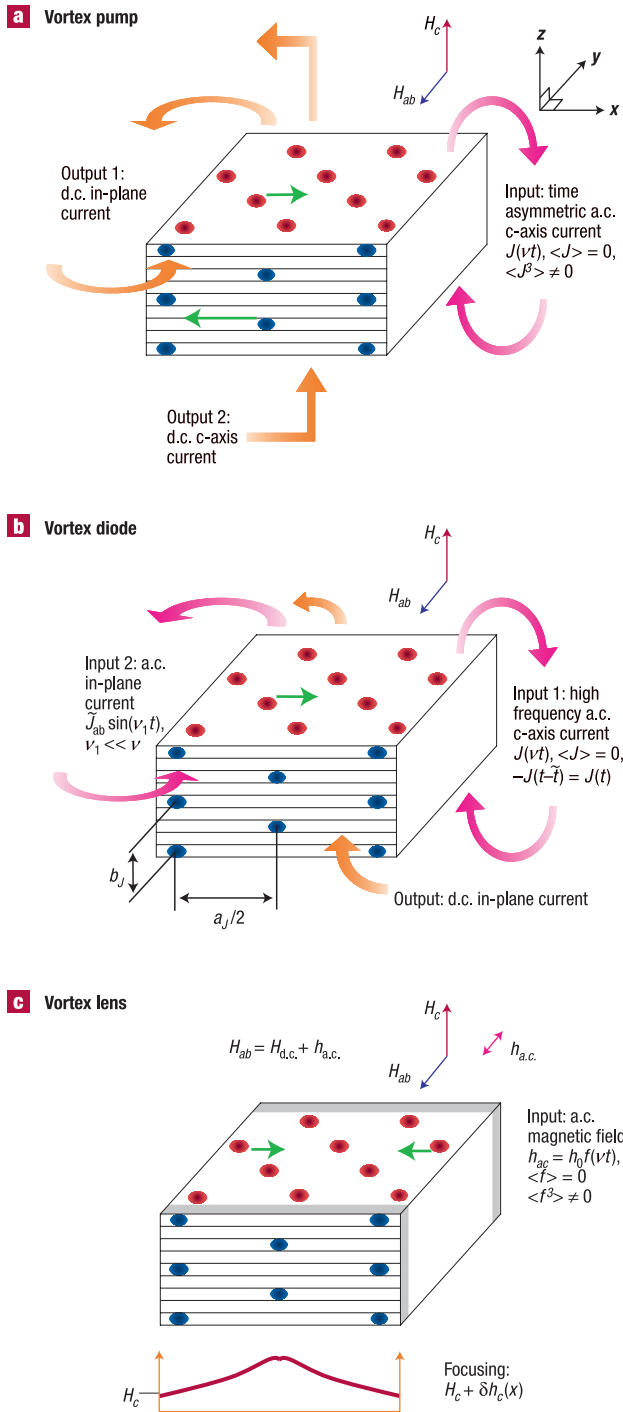
in the sample. This provides many advantages, including greatly simplifying the experimental set-up, and also the possibility of modifying at will the type of asymmetry generated inside the sample, because this is controlled by the time-dependent applied current or external field. In this context, we propose three different types of vortex devices (pump, diode and lens), shown in Fig. 1. The vortex pump in Fig. 1a uses an applied time-asymmetric a.c. current along the c axis to generate d.c. vortex motion. As sketched in Fig. 2, this vortex pump can operate in two different modes: (1) 'conveyor drag' mode, when the d.c. transport of both PVs and JVs is induced by the slow common motion of both PVs and JVs in the forward direction, followed by a fast backward jump of now free JVs which leave behind the unloaded PVs; and (2) stochastic 'ratchet' mode, where non-equilibrium thermal fluctuations of PV stacks are rectified by the asymmetric time-averaged potential generated by the oscillating JVs. This asymmetric potential can also be used for rectifying the deterministic low frequency a.c. motion of PVs in the vortex diode (Fig. 1b). The vortex lens (Fig. 1c) uses an applied time-asymmetric a.c. magnetic field to increase or decrease the PV density at the centre of the sample.

MUTUAL ATTRACTION OF PVs AND JVs

This mutual pinning can be estimated by considering the competition between the elastic force, reducing the bending of pancake stacks, and the bending-producing Lorentz force induced by the in-plane currents of the JVs[25,26]. Hence, the energy of a PV stack at a point x (z axis along the c axis and y axis along the JVs; see Fig. 1a) is determined by the energy functional $E[u_p] = \int dz[\tilde{U}_{44}u_p^2(x, z)/2 - (\Phi_0/c)j_J(x, z)u_p(x, z)]$. Here, u_p is the y-axis displacement of the PV from a straight line; $\tilde{U}_{44}$ is the tilt stiffness of the PV stack; and j_J is the in-plane current density associated with the JVs. In the presence of JVs, the (originally straight) PV stacks bend. Its new equilibrium state corresponds to the minimum of the energy functional E with respect to u_p, that is, the balance of the Lorentz and elastic forces. Because of the spatial variation of the in-plane JV currents $j_J(x)$, the energy $E_{PV}(x) = \min_{u_p}(E[u_p])$ of the bent PV stack depends on its location x within the JV sublattice. This results in the effective potential per PV: $\mathscr{U}(0 < x < a_J/2) = -\pi(s/b_J)^2\varepsilon_0\{\coth[\pi(\sqrt{3}x/a_J + s/b_J)] + \coth[\pi(\sqrt{3}/2 - \sqrt{3}x/a_J + s/b_J)]\}$, where $\varepsilon_0 = \Phi_0^2/(4\pi\gamma^2 s\ln(1 + \gamma H_{ab}\lambda_{ab}^2/\Phi_0))$ (ref. 25) is the energy scale of the PV–JV interaction, $a_J = (\sqrt{3}\Phi_0/2H_{ab})^{1/2}$ and $b_J = (2\Phi_0/\gamma\sqrt{3}H_{ab})^{1/2}$ are the in-plane and out-of-plane constants of the JV sublattice, Φ_0 the flux quantum, λ_{ab} the in-plane

tunable voltage transformer of perpendicular voltages U_c and U_{ab} along the c axis and along the JVs respectively. The voltage ratio $U_{ab}/U_c = H_c L/H_{ab}d$ can be tuned to an appropriate value by varying the in-plane H_{ab} and out-of-plane H_c magnetic fields, at fixed sample length L along the JVs, and c-axis thickness d. Since the ab-plane resistivity is quite low, our proposed voltage transformer might be easier to realize as a current transformer.

In this paper, we study how an a.c. (electrical or magnetic) driving can produce d.c. vortex transport without adding fixed pins in the sample. That is, there is no need to use either lithography, irradiation, or any other way to introduce a fixed spatial asymmetry
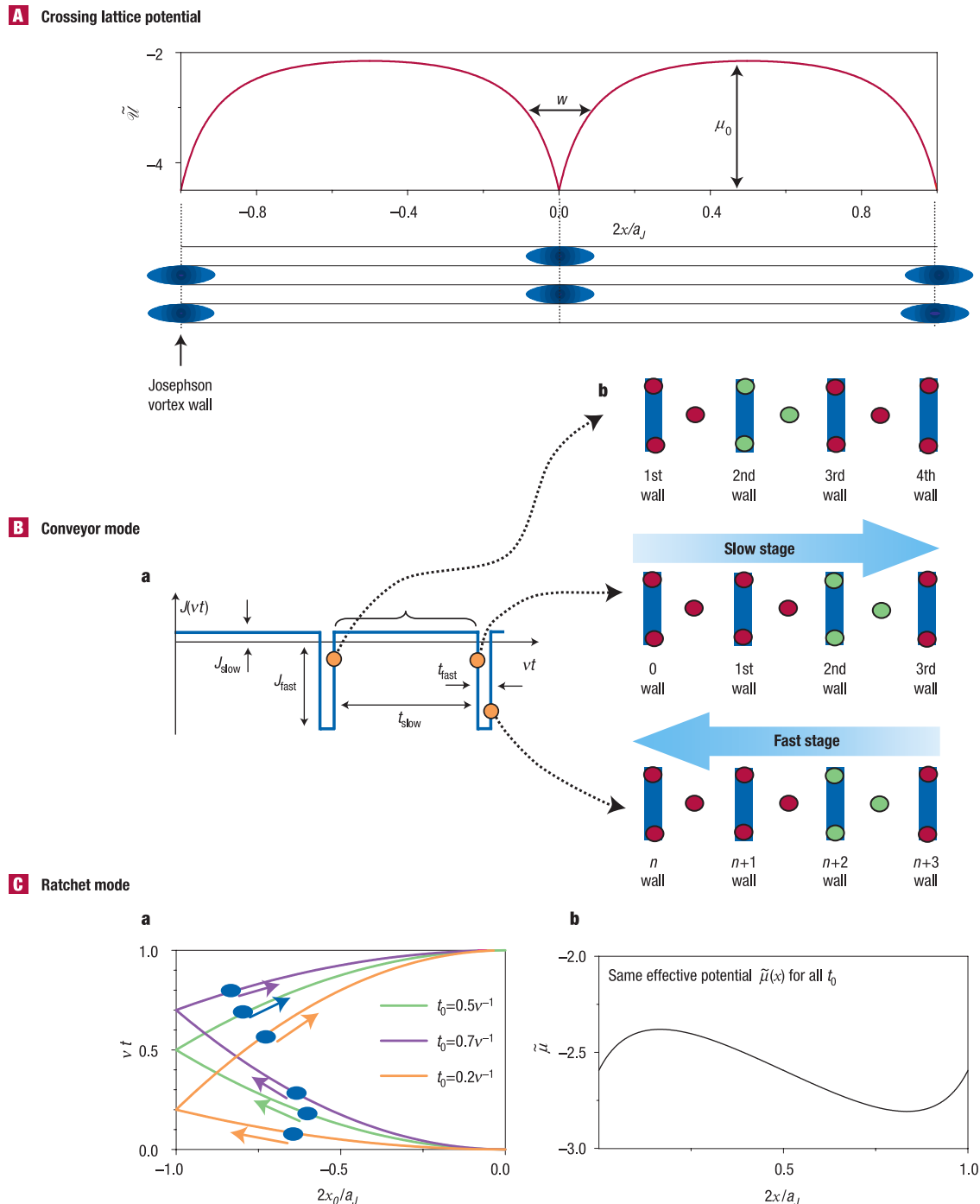
Figure 2 Modes of operation of the vortex pump. A Dimensionless potential energy $\tilde{\mathcal{U}} = \mathcal{U}/(\pi(s/b_J)^2\epsilon_0)$ felt by the PVs at different positions x with respect to the JV lattice where w is the effective width of the potential determined by the core of a JV. **B** The conveyor operating mode of the vortex pump. **B, a** shows an example of a strongly asymmetric zero-averaged input a.c. electrical current. **B, b** presents a sketch of how the vortex transport proceeds. The slow common motion of both PVs and JVs shifts the green PV stacks forward (to the right) on the first stage of the a.c. period, and the fast backward-moving JVs leave behind the PVs during the remaining part of the cycle. Relative PV–JV positions are shown at the moments flagged by the orange circles in the $J(\nu t)$ plot (B, a). Owing to a very anisotropic viscosity, the JVs shift further to the left than to the right. Thus, the JV walls marked as 1st, 2nd, 3rd, and 4th move to the left and different JVs (labelled here by n, $n+1$, $n+2$, and $n+3$) come into the displayed region. Repeating this process provides two opposite net d.c. motions involving both the PVs and the JVs. **C** Ratchet operating mode of the vortex pump. **C, a** presents the location x_0 (shown in the horizontal axis for convenience) of a JV wall plotted versus the dimensionless time νt during one cycle. Three examples are shown; two (orange and purple) are asymmetric in time. Note the larger velocity near $x_0 = 0$ for all trajectories. **C, b** shows the dimensionless 'effective' ratchet potential, $\tilde{\mu} = \mu/(\pi(s/b_J)^2\epsilon_0)$, felt by the PVs, obtained by time-averaging the PV–JV potential in **A** over the oscillations of the JVs shown in **C, a**. Remarkably, μ does not depend on the time asymmetry controlled by t_0.

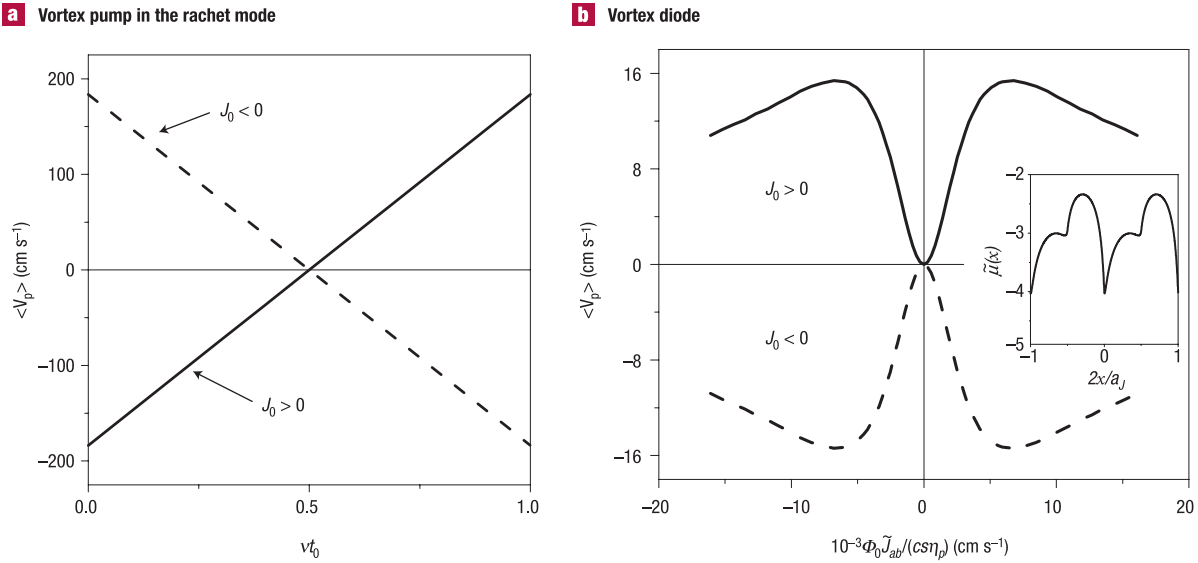**a** Vortex pump in the rachet mode

b Vortex diode

Figure 3 The motion of the PV stacks can be controlled by changing input parameters. a Net average PV velocity versus degree of time-asymmetry t_0, and **b** versus in-plane driving current amplitude $\tilde{J}_{ab}$ for the vortex pump (ratchet mode) and vortex diode, respectively. In the vortex pump (**a**), the net PV velocity can take a desired value by changing t_0 and/or the direction of the applied c-axis current, determined by its amplitude J_0. In the vortex diode (**b**), the inversion of the c-axis current inverts the net d.c. PV velocity, and its absolute value is controlled by the intensity $\tilde{J}_{ab}$ of the applied in-plane a.c. current. We have here chosen the following parameters: $H_c = 28\,\mathrm{Oe}$, $H_{ab} = 500\,\mathrm{Oe}$, $\gamma = 100$, $T = 30\,\mathrm{K}$, $T_c = 90\,\mathrm{K}$, $\nu = 1.4\,\mathrm{GHz}$, which are representative for $\mathrm{Bi_2Sr_2CaCu_2O_{8+\delta}}$. The inset shows an example of the time-averaged asymmetric potential $\tilde{\mu}(x)$ generated by symmetrically oscillating JVs with a time dependence given by $x_0 = a_J \sin^4(\nu t)/4$.

penetration depth, s the interlayer distance, and γ the anisotropy parameter. The washboard-type potential $\mathscr{U}(x)$ felt by the PVs (Fig. 2A) is periodic, with spatial period $a_J/2$, and potential-well depth of about $s\varepsilon_0/b_J$.

PANCAKE VORTEX PUMP

The pancake vortex pump in Fig. 1a converts the time-asymmetric oscillations of the JVs, induced by the time-asymmetric applied a.c. c-axis current, into a d.c. drift of both PVs and JVs. The overdamped oscillations, with frequency ν, of the JVs produce a swinging potential $\mathscr{U}(x - x_0(\nu t))$ for the PV stacks. The coordinate $x_0(t)$ of a chosen JV obeys $\eta_J\,dx_0/dt = (\Phi_0/c)J(\nu t)$; with zero time-averaged c-axis current density J ($\langle J \rangle \equiv \nu \int_0^{1/\nu} J(t)\,dt = 0$), viscous drag coefficient η_J, and speed of light c. There are two different working regimes, depending on the intensity of the a.c. driving current.

CONVEYOR BELT MODE

The simplest mechanism for the d.c. flux transport is based on the velocity-dependence of the drag of PVs by JVs. If the velocity V_{slow} of the forward-moving JVs is slow enough, the PV stacks remain trapped on the JVs and both move together to the right (during the slow-moving stage of Fig. 2B, b). In order to keep PVs pinned by JVs during this slow-moving stage, the viscous force slowing down the PVs has to be smaller than the maximum mutual pinning force $f_{pin} \sim \varepsilon_0/a_J$, that is, $\eta_p s V_{\mathrm{slow}} < f_{pin}$, with the viscous coefficient η_p per unit length of a PV stack. On the way back, the JVs must suddenly move fast (with velocity V_{fast} such that $\eta_p s V_{\mathrm{fast}} > f_{pin}$) in order to throw the PVs out of the JV–PV mutual potential wells and leave them behind (during the fast-moving stage of Fig. 2B, b). Thus, the PVs shift to the right and stick to other JVs at the beginning of the next period. Repeatedly cycling this motion provides a d.c. PV drift, which generates an in-plane d.c. electrical current.

Furthermore, the PV–JV common slow motion is more viscous ($\eta_J^{\mathrm{slow}} = \eta_J^{\mathrm{bare}} + \eta_p H_c/H_{ab}$) than the uncoupled fast motion of 'free' JVs leaving behind unloaded fixed PVs ($\eta_J^{\mathrm{fast}} = \eta_J^{\mathrm{bare}}$). Here, it is important to stress that there is a difference of about five orders of magnitude in the PV and 'bare' JV viscosities. These can be evaluated from the following equations $\eta_J^{\mathrm{bare}} \sim \Phi_0^2/(2\pi\gamma s^2 c^2 \rho_c)$ and $\eta_p \sim \Phi_0^2/(2\pi\xi_{ab}^2 c^2 \rho_{ab})$, where ρ_{ab} and ρ_c are the in-plane and out-of-pane normal state resistivities, and ξ_{ab} the in-plane coherence length. Therefore, the JVs feel an extremely anisotropic viscosity, which rectifies their own motion inducing an output c-axis d.c. electrical current. The d.c. velocities of the PVs and JVs can be evaluated as $\langle V_p \rangle \approx \Phi_0 J_{\mathrm{slow}}/c\eta_J^{\mathrm{slow}}$ and $\langle V_J \rangle \approx \Phi_0 J_{\mathrm{slow}}(1/\eta_J^{\mathrm{slow}} - 1/\eta_J^{\mathrm{fast}})/c$, for the strongly time-asymmetric a.c. input current densities J_{slow} and J_{fast} for the slow and fast stages. Here, the time asymmetry Γ can be measured by the ratio $J_{\mathrm{fast}}/J_{\mathrm{slow}} = t_{\mathrm{slow}}/t_{\mathrm{fast}} = \Gamma \gg 1$, with respective time intervals t_{slow}, t_{fast} (Fig. 2B, a). With increasing current at a fixed Γ, the d.c. PV and JV velocities monotonically increase until the PV–JV common slow velocity exceeds its maximum value $V_{\mathrm{slow}}^{\mathrm{max}} = f_{pin}/(\eta_p s)$, which happens at the depinning current density $J_{\mathrm{slow}} = J_{\mathrm{depin}} \sim c\varepsilon_0\eta_J^{\mathrm{slow}}/(a_J s\Phi_0\eta_p)$. At higher currents, $J_{\mathrm{slow}} > J_{\mathrm{depin}}$, the conveyor belt mode can be no longer sustained because the PVs cannot follow the JVs, even during the slow-moving stage.

RATCHET RECTIFIER

At high enough input current, $J_{\mathrm{slow}} > J_{\mathrm{depin}}$, the vortex pump operates in another mode—the ratchet rectifier—where thermal noise plays a key role in the net PV transport. In this working regime, the influence of the PVs on the high-frequency overdamped oscillations of JVs seems to be negligible. Nevertheless, the 'free' PVs still feel the time-averaged mutual potential energy $\mu(x) = \nu \int_0^{1/\nu} \mathscr{U}(x - x_0(\nu t))\,dt$, rather than its instant value. If such an effective potential μ is asymmetric in space, it rectifies the non-equilibrium thermal fluctuations of the PV stacks, producing a net

transport of PVs. The average potential μ at the point x is quite robust with respect to changes in the PV–JV interactions. Indeed, the potential $\mu(x)$ is essentially determined by how much time an energy well, with 'effective' width w and depth μ_0 (Fig. 2A), spends at that position. That is, $\mu(x) \approx -\mu_0 \nu[w/|\dot{x}_0^+(x)| + w/|\dot{x}_0^-(x)|]$, where $\dot{x}_0^+$ and $\dot{x}_0^-$ are the forward and backward velocities at which the well passes by x (for simplicity, we assume that the amplitude A of the JV oscillations is smaller than half of the interwell distance $a_J/4$). This estimate for $\mu(x)$ is consistent with the time-averaged potential $\mu(x)$ that has the spatially-asymmetric smooth 'sawtooth' shape (Fig. 2C, b) here with $A = a_J/4$. To obtain the potential shown in Fig. 2C, b, the time dependence of the oscillations was chosen as $x_0 = 2A\sqrt{t/t_0}$, for $0 < t < t_0$, and $x_0 = 2A\sqrt{(1-\nu t)/(1-\nu t_0)}$, for $t_0 < t < \nu^{-1}$ (see Fig. 2C, a). The JV turning-point time t_0 quantifies the degree of asymmetry with $t_0 = \nu^{-1}/2$ for the symmetric signal. The most pronounced ratchet potential can be achieved if the neighbouring potential wells do not overlap during the oscillation: $2A \lesssim a_J/2$. This inequality, $a_J/2 \gtrsim \int_0^{t_0} dt\, \Phi_0 J(\nu t)/(c\eta_J^{\mathrm{bare}}) \sim \Phi_0 \sqrt{\langle J^2 \rangle}/(\nu c \eta_J^{\mathrm{bare}})$, gives an estimate of the optimal frequency needed for the generation of a 'sawtooth-shaped' ratchet potential, $\nu_{\mathrm{optimal}} \sim \Phi_0 \sqrt{\langle J^2 \rangle}/(ca_J \eta_J^{\mathrm{bare}})$. Moreover, we find that the motion of PVs can be easily controlled (see Fig. 3a) by changing the temporal asymmetry or direction of the c-axis current (see Methods).

VORTEX DIODE

The vortex diode shown in Fig. 1b uses the ratchet potential generated by the oscillating JVs, which are driven by a high frequency c-axis current, to rectify the applied a.c. current $J_{ab} = \tilde{J}_{ab}\sin(\nu_1 t)$ flowing along the in-plane magnetic field (both along the y axis). Instead of a time-asymmetric c-axis current, previously needed for inducing a d.c. current in the vortex pump, now the rectification of the in-plane a.c. current in the vortex diode is only governed by $\mu(x)$. Indeed, the rectification for the vortex diode does not depend on the time asymmetry because the ratchet potential $\mu(x)$ does not depend on the turning-point time t_0 (Fig. 2C, b). In contrast, $\mu(x)$ reflects to $\mu(-x)$ when the c-axis current is inverted $J \to -J$, resulting in a sign change of the PV d.c. velocity in the vortex diode. It can be shown that the condition for generating d.c. PV motion through the vortex diode is $-J(t - \tilde{t}) \neq J(t)$ for an arbitrary time shift $\tilde{t}$. For instance, the time-symmetrical JV oscillations $x_0 \propto \sin^4(\nu t)$, which satisfies the last inequality, generate the time-averaged spatially asymmetric ratchet potential shown in the inset of Fig. 3b.

The physical concept underlying the vortex diode operation is somewhat different from the vortex pump in the 'ratchet' mode. The stochastic transport used in both devices requires a spatial asymmetry as well as a non-equilibrium state. The first condition, the breaking of the spatial symmetry, is realized by the oscillations of JVs in both devices. However, in contrast to the vortex pump, kept out of equilibrium by the asymmetric swinging of the mutual PV–JV potential, the vortex diode is kept out of equilibrium mostly by the applied a.c. in-plane current. Thus, the vortex diode can be considered as an a.c. tilting ratchet[4]. In such ratchets, the d.c. current does not go to zero when $T \to 0$ if a strong enough a.c. driving is applied. It shows that thermal fluctuations only support the d.c. motion, which is mostly governed by a deterministic a.c. force (associated here with the in-plane a.c. current).

The direction of the rectified current through the vortex diode can be easily changed by the inversion $J \to -J$ of the c-axis current, whereas the absolute value of the output d.c. PV velocity can be tuned by changing the intensity $\tilde{J}_{ab}$ of the in-plane a.c. drive (Fig. 3b and Methods). The vortex diode operates well if all relevant energy scales are of the same order, that is, $k_B T \lesssim \Delta\mu \equiv [\max(\mu(x)) - \min(\mu(x))]$, $\Phi_0 \tilde{J}_{ab} s a_J/2c \sim \Delta\mu$, giving the following estimates:

$T \lesssim 10\,\mathrm{K}$, $\tilde{J}_{ab} \sim 4\,\mathrm{kAmp\,cm}^{-2}$ at $H_{ab} \approx 300\,\mathrm{Oe}$, $\gamma = 100$, $s = 15\,\mathrm{\AA}$, and $\lambda = 2{,}000\,\mathrm{\AA}$.

VORTEX LENS

The vortex lens in Fig. 1c can be considered as two joined vortex pumps pushing vortices in opposite directions[7,9]. Two edges of the sample can be irradiated in order to increase pinning and to prevent the leakage of PVs along the direction of $\mathbf{H}_{ab}$. A possible operating mode of a vortex lens can be to slowly increase the in-plane field, from 0 to $H_{ab}^{\max}$, for a fixed value H_c of the out-of-plane magnetic field. The increasing ab magnetic field slowly drives JVs from the edges to the centre of the sample. In turn, JVs pin PVs and drag them along to the centre. As a result, PVs accumulate in the middle of the lens. The upper bound for the magnetic lensing efficiency can be estimated by considering the maximum PV density gradient kept by the JVs, that is, by equating the pinning force ε_0/a_J to the magnetic pressure $\Phi_0 s |h_1 - h_2|/4\pi\lambda_{ab}$ acting on a PV trapped by a JV (and trying to push the PV out of the well), with the out-of-plane magnetic fields h_1 and h_2 to the right and left of this JV wall. Therefore, the maximum c-axis field gradient towards the centre of the sample is about $|dH_c/dx|_{\max} \sim 8\pi\varepsilon_0\lambda_{ab}/\Phi_0 a_J^2 s$, corresponding to the critical current density $J_{\mathrm{crit}} \sim cH_{ab}\lambda_{ab}/4\pi\gamma^3 s^2 \sim 2\times10^5\,\mathrm{A\,cm}^{-2}$, for $\gamma = 300$, $\lambda_{ab} = 2{,}000\,\mathrm{\AA}$, $s = 15\,\mathrm{\AA}$ and $H_{ab} = 300\,\mathrm{Oe}$, for $\mathrm{Bi_2Sr_2CaCu_2O_{8+\delta}}$. In addition, the many PVs that are squeezed towards the centre of the sample prevent JVs from moving towards the centre. This, in turn, creates a gradient of JVs associated with the c-axis current $J_c \sim J_{ab}a_Jb_J/(\lambda_{ab}a_p)$, because $\partial H_{ab}/\partial x \sim \partial H_c/\partial x \cdot a_Jb_J/(\lambda_{ab}a_p)$.

If the superposition $H_{ab}(t) = H_{\mathrm{d.c.}} + h_{\mathrm{a.c.}}(t)$ of the d.c., $H_{\mathrm{d.c.}}$, and relatively weak time-asymmetric a.c., $h_{\mathrm{a.c.}}(t)$, magnetic fields is applied, the JVs are asymmetrically pulled in and pushed out of the sample. By analogy with the vortex pump, the time-asymmetric JV motion provides the PV transport either towards the centre of the sample (convex lens for PVs and concave lens for JVs) or towards the surface (opposite lensing effect). An important advantage of such an a.c.-driven vortex lens is that the switching between convex and concave PV lenses can be easily performed by changing the asymmetry of the applied a.c. field, such as $\nu \to -\nu$. The PV lens operates properly if the JVs move throughout the whole sample, that is, the sample size L is larger than the skin depth $\delta = c[\rho_c^\star(H)]^{1/2}/(2\pi\sqrt{\nu})$, where $\rho_c^\star$ is the measured c-axis resistivity. Thus, the maximum frequency of the a.c. magnetic field $h_{\mathrm{a.c.}}$ is about $\nu_{\max} = c^2\rho_c^\star/4\pi^2L^2 \sim 2\,\mathrm{GHz}$ for $\rho_c^\star = 1\,\mathrm{Ohm\,cm}$ and the sample length $L = 0.1\,\mathrm{cm}$ along the x axis.

Note, that the joint dynamics of the JVs and PVs discussed in this work can be very important for understanding a broad class of dynamical phenomena for $\mathrm{Bi_2Sr_2CaCu_2O_{8+\delta}}$ in tilted magnetic fields, especially close to the ab plane. These effects have recently begun to be studied experimentally[29–32], and a detailed theoretical analysis is still missing. For example unusual oscillations in the c-axis resistivity, followed by a sharp drop, have been found[30,31] when increasing a magnetic field oriented close to the ab plane. Because the mutual PV–JV attraction increases with the in-plane magnetic field ($f_{pin} \sim \varepsilon_0/a_J \propto \sqrt{H_{ab}}$), this behaviour could be attributed to a dynamical commensurate–incommensurate phase transition of the JV and PV lattices, that is, a succession of stick-slip partial trappings of PVs by JVs, followed by a complete trapping of PVs by JVs at high enough magnetic field, resulting in the low resistance common PV–JV motion.

In conclusion, we have proposed several experimentally realizable devices that can easily control the motion of magnetic flux quanta in very anisotropic superconductors, such as $\mathrm{Bi_2Sr_2CaCu_2O_{8+\delta}}$, and could be used in different types of micromagnetic machines. Combinations and extensions of these novel types of devices,

which use the PV–JV mutual potential, can achieve an unprecedented level of control of the transport of vortices, and effectively open the possibility of sculpting complex microscopic magnetic flux landscapes. These effects could be easily visualized by the local magnetic flux probes that have been developed, including Lorentz microscopy[13–17] scanning probes (including Hall[18,33], SQUID (superconducting quantum interference device) and scanning tunnelling microscopy), Hall arrays, and magneto optics[19,20,34]. Moreover, this radically new approach to control particle motion (without a fixed spatial asymmetry in the sample) is quite general, not restricted to crossing lattices, and applicable to any mixture of interacting particle species driven differently (for example, because of different magnetic moments or different charges) by the same a.c. time-asymmetric force.

METHODS

NET AVERAGE PANCAKE VORTEX VELOCITY

For a vortex pump working in the ratchet mode, the PV wandering induced by thermal noise can be studied by using the Fokker–Plank equation written for the PV stack density n: $\eta_p s \partial n/\partial t = \partial/\partial x \{\mathcal{U}'(x - x_0(t))n + k_B T \partial n/\partial x\}$, where k_B is the Boltzmann constant and T the temperature. In the high-frequency limit, we can expand the vortex current with respect to the reciprocal of the frequency ν, up to first order, and obtain an expression for the net PV velocity:

$$\langle V_P \rangle = \frac{l}{\eta_p s} \int_0^l dx \int_0^1 d\tau \left[\mathcal{U}''(x - x_0(\tau)) + \frac{(\mu'(x))^2}{k_B T} \right]$$
$$\times \left\{ \int_0^\tau \mathcal{U}'(x - x_0(\tilde{\tau})) d\tilde{\tau} - \tau \mu' \right\}$$
$$\times \left\{ \nu \int_0^l \exp\left(\frac{\mu(\tilde{x})}{k_B T}\right) d\tilde{x} \int_0^l \exp\left(-\frac{\mu(\tilde{x})}{k_B T}\right) d\tilde{x} \right\}^{-1}$$

(1)

with $\tau = \nu t$ and $l = a_J/2$ and the prime denotes a derivative: $' = \partial/\partial x$. In strong contrast to the temperature-independent vortex d.c. motion in the 'conveyor belt' mode, the net current (1) tends to zero as the temperature goes to zero for the 'ratchet rectifier' regime. This indicates that the non-equilibrium thermal noise drives the PV vortices in the latter mode, as opposed to the deterministic net vortex transport in the conveyor belt regime. According to (1), the net PV velocity depends linearly on the asymmetry time, $\nu^{-1}/2 - t_0$, and changes sign when switching the time asymmetry of the a.c. input current, for example, when $\nu \rightarrow -\nu$ or $t_0 \rightarrow \nu^{-1}/2 - t_0$. In addition, the PV velocity $\langle V_P \rangle$ also changes sign as the a.c. current is inverted $J \rightarrow -J$.

Now we consider the vortex diode case. If the frequency of the in-plane a.c. current flowing through the vortex diode is low enough, we can estimate the net d.c. PV velocity as

$$\langle V_P \rangle = \frac{\nu_1}{\eta_p s} \int_0^{\nu_1^{-1}} dt \frac{k_B T l(1 - \exp(-F(t)l/k_B T))}{\int_0^l dx \int_x^{l+x} dy \exp[(\mu(y) + F(t)x - \mu(x) - F(t)y)/k_B T]}$$

(2)

by applying the adiabatic approximation[35] to the Fokker–Planck equation having the a.c. tilting ratchet potential as $\mu(x) - F(t)x$; where the a.c. Lorentz force per PV is $F(t) = \Phi_0 \tilde{J}_{ab} s \sin(\nu_1 t)/c$.

References

1. Astumian, R. D. Making molecules into motors. *Sci. Am.*, 56–64 (July 2001).
2. Hänggi, P. & Reimann, P. Quantum ratchets reroute electrons. *Phys. World* **12,** 21–22 (1999).
3. Linke, H. Ratchets and brownian motors: Basics, experiments and applications. *Appl. Phys. A (Special Issue)* **75,** 167 (2002).
4. Reimann, P. Brownian motors: noisy transport far from equilibrium. *Phys. Rep.* **361,** 57–265 (2002).
5. Jülicher, F., Ajdari, A. & Prost, J. Modeling molecular motors. *Rev. Mod. Phys.* **69,** 1269–1282 (1997).
6. Astumian, R. D. Thermodynamics and kinetics of a Brownian motor. *Science* **276,** 917–922 (1997).
7. Wambaugh, J. F., Reichhardt, C., Olson, C. J., Marchesoni, F. & Nori, F. Superconducting fluxon pumps and lenses. *Phys. Rev. Lett.* **83,** 5106–5109 (1999).
8. Lee, C.-S., Jankó, B., Derényi, I & Barabási, A.-L. Reducing vortex density in superconductors using the 'ratchet effect'. *Nature* **400,** 337–340 (1999).
9. Olson, C. J., Reichhardt, C., Jankó, B. & Nori, F. Collective interaction-driven ratchet for transporting flux quanta. *Phys. Rev. Lett.* **87,** 177002 (2001).
10. Nori, F. Intermittently flowing rivers of quantized magnetic flux. *Science* **271,** 1373–1374 (1996).
11. Gammel, P. Why vortices matter. *Nature* **411,** 434–435 (2001).
12. Avraham, N. *et al.* 'Inverse' melting of a vortex lattice. *Nature* **411,** 451–454 (2001).
13. Harada, K. *et al.* Direct observation of vortex dynamics in superconducting films with regular arrays of defects. *Science* **274,** 1167–1170 (1996).
14. Tonomura, A. *et al.* Motion of vortices in superconductors. *Nature* **397,** 308–309 (1999).
15. Tonomura, A. *et al.* Observation of individual vortices trapped along columnar defects in high-temperature superconductors. *Nature* **412,** 620–622 (2001).
16. Matsuda, T. *et al.* Oscillating rows of vortices in superconductor. *Science* **294,** 2136–2138 (2001).
17. Tonomura, A. *et al.* Observation of structures of chain vortices inside anisotropic high-T_c superconductors. *Phys. Rev. Lett.* **88,** 237001 (2002).
18. Grigorenko, A., Bending, S., Tamegai, T., Ooi, S. & Henini, M. A one-dimensional chain state of vortex matter. *Nature* **414,** 728–731 (2001).
19. Vlasko-Vlasov, V. K., Koshelev, A., Welp, U., Crabtree, G. W. & Kadowaki, K. Decoration of Josephson vortices by pancake vortices in $Bi_2Sr_2CaCu_2O_{8+\delta}$. *Phys. Rev. B* **66,** 014523 (2002).
20. Tokunaga, M., Kobayashi, M., Tokunaga, Y. & Tamegai, T. Visualization of vortex chains in $Bi_2Sr_2CaCu_2O_{8+y}$ by magneto-optical imaging. *Phys. Rev. B* **66,** 060507(R) (2002).
21. Ooi, S., Shibauchi, T., Itaka, K., Okuda, N. & Tamegai, T. Vortex matter transition in $Bi_2Sr_2CaCu_2O_{8+y}$ under tilted fields. *Phys. Rev. B* **63,** 20501(R) (2001).
22. Ooi, S., Shibauchi, T., Okuda, N. & Tamegai, T. Novel angular scaling of vortex phase transitions in $Bi_2Sr_2CaCu_2O_{8+y}$. *Phys. Rev. Lett.* **82,** 4308–4311 (1999).
23. Mirković, J., Savel'ev, S. E., Sugahara, E. & Kadowaki, K. Stepwise behavior of vortex-lattice melting transition in tilted magnetic fields in single crystals of $Bi_2Sr_2CaCu_2O_{8+\delta}$. *Phys. Rev. Lett.* **86,** 886–889 (2001).
24. Bulaevskii, L. N., Ledvij, M. & Kogan, V. G. Vortices in layered superconductors with Josephson coupling. *Phys. Rev. B* **46,** 366–380 (1992).
25. Koshelev, A. E. Crossing lattices, vortex chains, and angular dependence of melting line in layered superconductors. *Phys. Rev. Lett.* **83,** 187–190 (1999).
26. Savel'ev, S. E., Mirković, J. & Kadowaki, K. London theory of the crossing vortex lattice in highly anisotropic layered superconductors. *Phys. Rev. B* **64,** 094521 (2001).
27. Buzdin, A. & Baladié, I. Attraction between pancake vortices in the crossing lattices of layered superconductors. *Phys. Rev. Lett.* **88,** 147002 (2002).
28. Dodgson, M. J. W. Phase transitions in isolated vortex chains. *Phys. Rev. B* **66,** 014509 (2002).
29. Latyshev, Yu. I., Gaifullin, M. B., Yamashita, T., Machida, M. & Matsuda, Y. Shapiro step response in the coherent Josephson flux flow state of $Bi_2Sr_2CaCu_2O_{8+\delta}$. *Phys. Rev. Lett.* **87,** 247007 (2001).
30. Hirata, K., Ooi, S., Sadki, E. H. & Mochiku, T. Josephson vortex flow in $Bi_2Sr_2CaCu_2O_{8+y}$. *Physica C* (in the press).
31. Ooi, S., Mochiku, T. & Hirata, K. Periodic oscillations of Josephson-vortex flow resistance in $Bi_2Sr_2CaCu_2O_{8+y}$. ArXiv.org: cond-mat/0112209.
32. Gaifullin, M. B., Latyshev, Yu. I., Yamashita, T. & Matsuda, Y. Shapiro step response in the vortex state of $Bi_2Sr_2CaCu_2O_{8+\delta}$. *Physica C* (in the press).
33. Field, S. B. *et al.* Vortex configurations, matching, and domain structure in large arrays of artificial pinning centers. *Phys. Rev. Lett.* **88,** 067003 (2002).
34. Indenbom, M. V. *et al.* Magneto-optical observation of twisted vortices in type-II superconductors. *Nature* **385,** 702–705 (1997).
35. Bartussek, R., Hänggi, P. & Kissner, J. P. Periodically rocked thermal ratchets. *Europhys. Lett.* **28,** 459–464 (1994).

Competing financial interests

The authors declare that they have no competing financial interests.